High-Resolution PET Imaging and Quantitation of Pharmaceutical Biodistributions in a Small Animal Using Avalanche Photodiode Detectors

C.J. Marriott, J.E. Cadorette, R. Lecomte, V. Scasnar, J. Rousseau and J.E. van Lier

Department of Nuclear Medicine and Radiobiology, Université de Sherbrooke, Sherbrooke, Québec, Canada

The feasibility of high-resolution PET using BGO-avalanche photodiode detectors for in vivo imaging and quantitation of the biodistribution of radiopharmaceuticals in small animals is demonstrated. A prototype PET camera consisting of two scanning arrays of eight EG&G C30994 solid-state scintillation detectors was used to simulate a 310-mm diameter dual-ring animal tomograph having a 130-mm port and three imaging slices, each about 3.5 mm thick. The spatial resolution (FWHM) is 3 mm or less, isotropic and uniform throughout the 120-mm diameter field of view. **Methods:** Female Fischer 344/CRBL rats implanted with subcutaneous mammary adenocarcinoma tumors were injected with copper-tetrasulfophthalocyanine ($CuPcS_4$), a potential sensitizer for the photodynamic therapy of cancer, labeled with ^{64}Cu ($T_{1/2}$ = 12.7 hr, β^+: 19%). **Results:** In spite of the low specific radioactivity of ^{64}Cu and other inherent limitations, organs such as the liver, kidneys and the tumor could be resolved with sufficient detail for their separation and quantitation. Apart from the tumor, agreement was obtained between the biodistributions measured by PET and by scintillation counting. The discrepancy for the tumor measurement results from averaging the radioactivity over the entire tumor volume when, in fact, $CuPcS_4$ does not completely penetrate the tumor. This incomplete penetration is noted on the PET images. **Conclusions:** PET based on avalanche photodiode detectors provides an accurate measurement of target organ and tumor tissue concentrations. These preliminary results demonstrate the potential of very high resolution PET for biodistribution studies in small animals.

Key Words: PET imaging; biodistribution; photodiode detectors; laboratory animals

J Nucl Med 1994; 35:1390–1397

Before new pharmacological agents can be administered to humans, it is necessary to develop and test protocols and evaluate the effects of the drug on biochemistry, metabolism and physiology in an animal model. Of particular interest is the study of the biodistribution and kinetics of substances such as drugs for other applications (*1,2*). Traditionally, these have been determined using radiolabeled tracers by dissection studies followed by gamma or liquid scintillation counting and autoradiography (*3*). Such an approach, however, is tedious and requires a large number of animals to ensure the reproducibility and reliability of the results.

The continuing development of high-resolution PET scanners for small animals and the availability of suitable isotopes (e.g., ^{11}C and ^{18}F) are providing an alternative which simplifies considerably the measurement and the development of models for the kinetics and distribution of tracer compounds (*4,5*). PET has many advantages, including significantly reducing the number of animals required for time-distribution studies, facilitating the monitoring of rapid changes in distributions, and making true in vivo distribution measurements feasible. The use of small animals facilitates manipulation and reduces the quantities of the substances required; it also helps reduce errors due to slight procedural differences and natural interanimal variations since the study can be repeated in the same animal several times (*6*).

The interest of this PET-based approach is demonstrated by the recent development of a number of specialized small animal systems (*7–10*). The most stringent requirement for quantitative dynamic imaging of small laboratory animals by PET is spatial resolution. The current technology using block detectors with crystal coding to the photomultiplier tubes (PMTs) impedes further improvement of the resolution beyond the 3–4 mm FWHM currently achievable.

A new technological approach using discrete detectors based on avalanche photodiodes (*11,12*) achieves very high resolution over a small field of view (FOV) making this approach ideal for animal imaging (*13,14*). This approach has the additional advantage of producing images virtually free of spatial distortion and permits very high count rates, with minimal loss due to pulse pile-up and deadtime. The first PET scanner based on avalanche photodiode detectors is currently being built in this laboratory and will shortly become available for animal studies (*15*). Table 1 presents the physical description and imaging characteristics of this instrument.

As the techniques and the apparatus improve, it is be-

Received Aug. 6, 1993; revision accepted Feb. 15, 1994.

For correspondence and reprints contact: Roger Lecomte, PhD, Department of Nuclear Medicine and Radiobiology, Faculté de médecine, Université de Sherbrooke, Sherbrooke, QC, Canada J1H 5N4.

TABLE 1
Physical Description and Performance Characteristics of the Sherbrooke Animal Tomograph Simulated in this Study

Detector type	EG&G C30994 Dual BGO/avalanche photodiode
BGO crystal size	3 × 5 × 20 mm (beveled)
Module dimension	3.8 × 13.2 × 33 mm
BGO crystal spacing	3.8 mm tangentially 5.5 mm axially
Number of detectors	256/ring
Number of detector rings	2 (1 layer of modules)
Ring diameter	310 mm
Port diameter	135 mm
Useful field-of-view	118 mm
Axial field	10.5 mm
Reconstruction planes	3 (2 direct, 1 cross)
Intrinsic spatial resolution (center)	
Transaxial	1.9 mm FWHM, 3.5 mm FWTM
Axial	3.1 mm FWHM, 5.4 mm FWTM
Reconstructed resolution*	2.1 mm FWHM, 3.9 mm FWTM
Sensitivity (11 cm∅ flood, 350 keV)	3.3 kcps/μCi/ml
Energy resolution	≤25% FWHM (511 keV)
Timing resolution	20 ns FWHM
Timing window	20 to 40 ns

*With dual position sampling.

coming possible to apply these PET techniques to study animal models of some very significant human diseases (*16*). One such field is oncology where the evaluation of tumor markers (*17–20*) is generating considerable interest. In this paper, by comparing quantitative data obtained with a simulator of the avalanche photodiode PET camera we demonstrate the capabilities and advantages of the PET approach for the in vivo quantitation of the biodistribution of a class of compounds with possible photodynamic cancer therapy applications.

MATERIALS AND METHODS

Animal Model

The animals selected and used for the experiments were Fischer 344/CRBL female rats implanted with the 13762 mammary adenocarcinoma (MAC). In total, eight rats were used for the experiment, one for the PET study and the remainder for dissection and scintillation-counting studies. A target weight of 150 g was fixed for the experiment as this corresponds to the largest rat which can be placed longitudinally in the field of view of the Sherbrooke PET simulator set up to simulate the small animal tomograph presently being assembled. It should be noted that much larger animals can be positioned transversely. Three weeks before the experiment, the peritonea of two rats were inoculated with the MAC cells and incubated for 7 days in ascite form. At the end of the incubation period these rats were killed, the ascite fluid recovered and the tumor cells isolated according to the usual protocol. A suspension of 11×10^5 cells in 0.05 ml of physiological saline was injected subcutaneously into the left flanks so as to lie in the plane chosen for tomography. For two of the rats, the concentration of the cell suspension was doubled. The subcutaneous tumors were then incubated for 14 days. As this is somewhat longer than the usual 10-day incubation period, the centers of the tumors were inadequately perfused and became necrotic. At the time of the experiments, the average tumor volume was 1.4 ± 0.5 ml. At the end of the incubation period, the animals weighed 150 ± 13 g, with some of them being much below the predicted weight because of their tumor burden.

During the incubation period, the rats were given food and water ad libitum. The animal experiments were carried out in accordance with the recommendations of the Canadian Council on Animal Care and the.In-house Ethics Committee for Animal Experiments.

Radioisotopes

Among the few isotopes suitable for imaging with the PET simulator, ^{64}Cu (*21,22*) ($T_{1/2}$ = 12.7 hr) was chosen because of its commercial availability (Dupont/NEN Products) and a half-life sufficiently long for delivery, chemistry and image acquisition with only a partial detector ring. Copper-64, however, has a number of disadvantages. The first is its low branching ratio to positron emission (19%) and the second is the very low specific radioactivity available. Before starting the chemistry for the labeling of H_2PcS_4, the specific activity was only 2.3 mCi/mg of Cu, or approximately 0.6 ppm of ^{64}Cu.

Chemistry

We used a metallo, tetrasulfonated phthalocyanine (PcS_4) as a tracer. The phthalocyanines are a group of compounds which have received much interest as photosensitizers for photodynamic cancer therapy (*23,24*). As their biological properties are beginning to be reasonably well elucidated, some prior estimation of tissue distribution was possible (*25–27*). For tracer applications, phthalocyanines have the advantage of being able to chelate a variety of metal ions, including copper, and of being relatively nontoxic. In addition, the chemistry required for labeling is straightforward and rapid. The tetrasulfonated form was chosen as it has somewhat higher tumor and kidney uptake and somewhat lower liver and spleen uptake than differently substituted analogs (*25*).

From previous experience with other metal chelates of sulfonated phthalocyanines, it is known that these compounds are not significantly degraded in vivo, much being excreted unmetabolized in the urine (*28,29*). Consequently, the radioactive ^{64}Cu remains bound to the phthalocyanine and therefore the level of tissue radioactivity can be assumed to be an accurate measure of the $CuPcS_4$ biodistribution.

Metal-free H_2PcS_4 was prepared by the condensation method of Weber and Busch (*30*) with the omission of phtalic acid from the mixture. The $[^{64}Cu]CuPcS_4$ was prepared via the direct insertion of an atom of copper into the metal-free H_2PcS_4, according to the substitution reaction:

$$Cu^{2+} + H_2PcS_4 \rightarrow 2H^+ + CuPcS_4. \qquad \text{Eq. 1}$$

For the biodistribution studies, 200 μl of $[^{64}Cu]Cu(NO_3)_2$ were evaporated to dryness. The residue was dissolved in 80 ml of N,N-dimethylformamide (DMF) and the pH was adjusted to 7.4 by the addition of 1 *M* HCl. This pH level is important to ensure a high labeling efficiency. Then 151.2 mg (181.5 μmole) of H_2PcS_4 in 8 ml of physiological saline were added and the reaction mixture refluxed at 130°C for 10 min. It was then evaporated to dryness to yield a dark blue powder. The radioactive powder was dissolved in 8 ml of physiological saline and filtered through a 0.45-μ membrane filter to remove any aggregates for injection into the rats. The specific activity was 26.3 μCi per mg $[^{64}Cu]CuPcS_4$ and no

purification was necessary as the radiochemical purity was higher than 94%, as assayed by thin-layer chromatography. The total time for labeling was under 1 hr.

The solution was prepared to ensure the highest possible specific radioactivity by the same procedure for the tomographic study. The difference was in the use of excess $^{64}Cu(NO_3)_2$. The unreacted ^{64}Cu was removed by passing the radioactive solution in a sodium citrate buffer (pH 5) through a reverse-phase SEP-PAK C-18 cartridge attached to a 10-ml plastic syringe at a flow rate of 5 ml · min^{-1}. The eluate containing unreacted ^{64}Cu was discarded and the blue radioactive product retained on the cartridge was washed with water (5 ml) and then eluted with 2 ml of DMF. The solvent was evaporated and the dark blue residue was dissolved to saturation (9 μmole · ml^{-1}) in 8 ml of physiological saline. Before injection, this solution was also filtered through a 0.45-μ membrane filter to remove any aggregates. The specific radioactivity was 104.6 μCi per mg [^{64}Cu]$CuPcS_4$ and the radiochemical purity was better than 94%.

Injection

Prior to the injection of the [^{64}Cu]$CuPcS_4$ solution, the rats were heparinized (Hepalean) to facilitate bleeding, anesthetized intramuscularly with a mixture of Xylozine (13 mg/kg) and Ketanine (85 mg/kg), and catheterized in the tail vein. The dose of filtered [^{64}Cu]$CuPcS_4$ solution injected into each animal was 0.5 ml, which had previously been demonstrated to be nonlethal. This was chased by approximately 0.3 ml of physiological saline to ensure that the entire volume of [^{64}Cu]$CuPcS_4$ solution was injected. Thus, a radioactivity of 438 μCi was injected into the rat for the PET measurement and a radioactivity of 110 μCi was injected into the other rats. Although the specific radioactivity of the two solutions differed by a factor of 4, the total concentration of $CuPcS_4$, both radioactive and nonradioactive, was identical. Consequently, the physiological properties of the two solutions were also identical, and comparison between the two methodologies was possible. To permit comparison, all activities mentioned in the remainder of this article are referred to as the time of injection of the rat for tomography.

Scintillation Counting

At the end of the distribution period (1 or 24 hr), the anesthetized animals were bled by cutting the left axillary artery and killed by exposing and opening the heart. The bleeding was necessary to maintain consistency between the scintillation and PET scanning procedures. It also ensured that the true tissue uptake without an additional contribution from blood was measured. The blood was recovered to measure the distribution of the [^{64}Cu]$CuPcS_4$. The other organs were then dissected out, and placed in pre-weighed test tubes. These tubes were sealed to prevent loss of moisture, weighed and left for over 24 hr to allow the radioactivity to decay enough for scintillation counting without detector saturation. The radioactivity in each tissue sample was counted in a LKB WALLAC 1282 Compugamma Universal Gamma Counter (Turku, Finland) using an energy window of 410–620 keV. These results were calibrated with respect to the radioactivity in a known volume (50 μl or 11 μCi) of the injected solution and the specific radioactivities (counts per minute per gram of tissue) were expressed as a percentage of the total injected dose.

PET Acquisition and Analysis

The PET images were obtained with the help of the Sherbrooke PET simulator of which a detailed description can be found elsewhere (*31*). The instrument was set up to simulate the animal PET system described in Table 1. One hour after the injection, the rat injected with 438 μCi of ^{64}Cu was anesthetized, decapitated and bled. The rat was killed to prevent redistribution of the tracer during the several hours required for the measurement. It was also important that the rat be bled to prevent the blood from gradually pooling in the lowest lying parts of the body. The rat was mounted on the PET simulator so that the plane containing the organs most likely to accumulate the [^{64}Cu]$CuPcS_4$, including portions of liver, kidneys and lungs was imaged. From prior dissection studies, the plane chosen for imaging was found to have its base about 0.8 cm from the dorsal surface of a 150-g rat. In order to validate the position of the imaged plane, lateral and anterior planar views were obtained with the PET prototype at the end of the tomographic acquisition. These measurements were also intended to evaluate the positioning accuracy in localizing regions of interest (ROI) from a fast full-body scan. The planar views were produced by scanning the specimen using the appropriate combination of scanning detector array and animal angular and axial positions. With a full ring of detectors, this would be equivalent to extracting two orthogonal planar views from the sinograms of a full-body scan.

Calibration markers consisting of sealed capillary tubes of an inside diameter of 1.4 mm containing [^{64}Cu]$CuPcS_4$ solution of 222 μCi/ml of radioactivity, were placed at the edge of the FOV in an equilateral triangular configuration with an edge length of 9.8 cm. As the calibration markers contain [^{64}Cu]$CuPcS_4$, their radioactivity decays in proportion to the decay of the radioactivity in the rat, thus simplifying quantitation of relative values of radioactivity.

The tomographic acquisition with the Sherbrooke PET simulator required a series of 144 sequential measurements in predetermined positions of the detector arrays and object (*31*). The rat was imaged for 4 min in the first array position. As the radioactivity decayed, the counting time for each array position was increased. The 144 different configurations required a total acquisition time of 14 hr. Data were acquired in the three adjacent planes defined by the two layers of detectors in the arrays. The second slice, composed of cross-projection data between the upper and lower detector planes, has twice the sensitivity of the other two direct planes.

The images were reconstructed by filtered backprojection using a ramp filter with a cutoff frequency of 5.3 cm^{-1}. Data points were interpolated to permit reconstruction on a 256 × 256 grid with pixel size of 0.48 mm × 0.48 mm. As count rates were low, there was no need to correct for deadtime, but correction was made for the differences in detector efficiencies, as described elsewhere (*31*). As the Sherbrooke PET simulator is not equipped for measuring the attenuation for each projection, the attenuation was not corrected during the reconstruction process. Nevertheless, a correction was introduced in the quantitation analysis as follows. A phantom having the same shape and dimensions as the rat was fabricated. Images of a ^{22}Na line source (0.25 mm diameter) were acquired at various locations corresponding to the organ's position with the phantom empty and filled with water. The attenuation correction factors for the various organs were estimated from the ratio of counts registered with and without water in the phantom. The attenuation for the calibration markers was also measured in the same way. Since the count rate from the calibration markers is also affected by attenuation, the overall effect of the attenuation correction is relatively small (<10%) on the measured radioactivity in the organs.

The levels of radioactivity in each organ were evaluated by

TABLE 2
Distribution of [^{64}Cu]CuPcS$_4$ in the Tissues of the Rats One Hour and 24 Hours After Injection*

	Biodistribution 1 hr postinjection (n = 3)		Biodistribution 24 hr postinjection (n = 4)	
Tissue	%ID/g	μCi/mg (10^{-2})	%ID/g	μCi/mg (10^{-2})
Blood	4.4 ± 0.5	1.9 ± 0.2	0.11 ± 0.01	0.048 ± 0.004
Tumor	0.36 ± 0.04	0.16 ± 0.02	0.63 ± 0.09	0.28 ± 0.04
Skin	0.2 ± 0.03	0.09 ± 0.01	0.14 ± 0.02	0.061 ± 0.009
Muscle	0.14 ± 0.05	0.06 ± 0.02	0.09 ± 0.01	0.039 ± 0.003
Spleen	2.3 ± 0.3	1.0 ± 0.1	4.08 ± 0.4	1.8 ± 0.2
Kidneys	4.9 ± 1.5	2.1 ± 0.6	6.9 ± 0.7	3.0 ± 0.3
Liver	3.9 ± 0.4	1.7 ± 0.2	7.6 ± 1	3.3 ± 0.5
Heart	1.1 ± 0.3	0.5 ± 0.1	0.38 ± 0.04	0.17 ± 0.02
Lungs	2.7 ± 0.7	1.2 ± 0.3	1.7 ± 0.3	0.7 ± 0.1
Eyes	0.36 ± 0.1	0.16 ± 0.05	0.18 ± 0.02	0.079 ± 0.009
Brain	0.07 ± 0.01	0.030 ± 0.004	0.01 ± 0.005	0.004 ± 0.02

*Activities are expressed as a percentage of the injected dose per gram (%ID/g) and in terms of the radioactivity normalized relative to the dose used for PET imaging (μCi/mg).

comparison with the calibration reference markers after correction for attenuation. As the size of the markers was less than the in-plane resolution, their diameter (~3.5 mm FWHM) as measured on the image was larger than the true diameter. To compensate for this partial volume effect and to account for resolution spillover, the calibration factor (counts per μCi in the image) was calculated from the total number of counts in a region of about 6 mm in diameter centered on the marker. With this calculation, the calibration factor between the number of counts in a region of the reconstructed image and the actual activity within the same region of the rat was found to be 270 counts/μCi for the two direct slices and 540 counts/μCi for the cross-slice.

The largest ROI, which could be defined avoiding the edges, was circumscribed for each organ. The number of counts in the ROI was determined and corrected for attenuation in the corresponding organ. The average radioactivity in each voxel was then calculated. As the smallest dimension of the organs measured was about 6 mm, the ROIs had a smallest dimension of the same order, large enough to avoid partial volume effects. The measurement was repeated for each of the organs in the three planes. The average of the measurements for the same organ were calculated and the overall uncertainty estimated as the standard deviation.

RESULTS

Scintillation Counting

The results for the biodistribution study are presented in Table 2 both as a percent of the injected dose and normalized relative to the radioactivity initially injected into the rat for the PET measurement. The errors are the standard deviations between the samples taken from each rat. After 1 hr the blood levels of [^{64}Cu]CuPcS$_4$ are still very high and the zones of greatest radioactivity are in the kidneys and liver. In comparison, the tumor uptake is relatively poor. After 24 hr the tumor uptake has increased, as has the uptake in the spleen, kidneys and liver.

PET Imaging

Despite the small size of the 150-g tumor-bearing rat and the difficulties inherent in experiments with the PET simulator which significantly limit the total number of counts, we are able to distinguish the two kidneys, the liver, a portion of lung and a well separated tumor on the left flank. These are illustrated in Figures 1 and 2. The left kidney, as it is confined to slice 3, is clearly seen to be more dorsal than the right one. The contrast, defined by the ratio of the radioactivity per pixel in the region of maximum radioactivity-to-the background radioactivity was 8.4. As the middle slice (slice 2) is reconstructed from the two cross-planes, its statistics are improved and the noise is reduced with respect to the other slices. To verify the accuracy of the image features, the rat used for tomography was dissected at the end of the experiment and the position of the

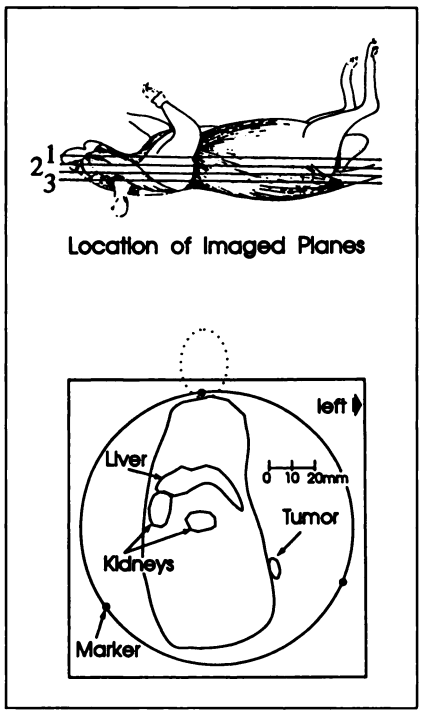

FIGURE 1. Position and numbering of the slices (above) and the position of the organs as determined by dissection of the animal at the end of the experiment (below). Each slice is assumed to be 3.5 mm thick.

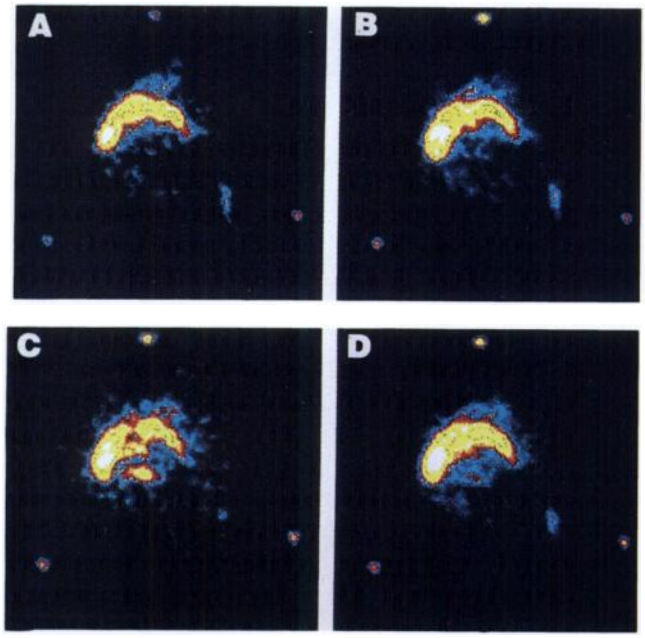

FIGURE 2. Images obtained with the PET simulator. (A) Slice 1; (B) Slice 2; (C) Slice 3; (D) summed image obtained by combining the three slices into a single 10.5-mm slice.

imaged structures compared and found to be compatible. The left kidney is somewhat more medial than normal as the rat's torso was not straight when mounted on the PET simulator. During dissection, the tissues observed to have high activity were observed to have taken on the blue color of the $CuPcS_4$.

From Table 2, one might expect to see the heart, the spleen, and from the usual high urine concentrations of water-soluble molecules, the bladder contents. The heart and the bladder, lying anteriorly, are not contained in the imaged planes. The spleen, although having a high radioactivity per gram, is a thin organ with an orientation relative to our imaging planes which is prone to partial volume effects. For the tumor, the activity is found to lie in a thin band on its outer edge. As the tumor was inoculated in the flank, it becomes smaller as one passes from slice 1 to slice 3.

Comparison of Scintillation and PET Biodistributions

To permit comparison of the scintillation counting and PET biodistributions it was assumed that all tissues had a density of 1 g/cm^3. In addition, the biodistribution doses expressed as a percentage of injected dose were expressed in terms of the radioactivity injected into the rat used for the PET scan (438 μCi). The results obtained by the two methods for the kidneys, liver, lung and tumor uptake are summarized in Table 3. For other organs, either the radioactivity was too low, they were not in the planes of the images, or they were of insufficient dimension in the image plane to be adequately resolved. It was estimated that approximately 20% of the total radioactivity injected remained within the imaged planes, principally in the liver and kidneys.

DISCUSSION

The difficulties inherent in the present experiment were considerable: low specific radioactivity, low branching ratio for positron emission, a limited total volume of [^{64}Cu] $CuPcS_4$ injected, and absence of a complete ring of detectors for PET data acquisition. The tracer constraints alone are responsible for at least a tenfold penalty in sensitivity, as compared to the usual PET tracers (e.g., ^{18}F) which can be produced carrier-free. Phthalocyanines are also not as specific markers as other more routine tracers. The incomplete ring is the most important limitation, however, as simulation of the entire ring requires 144 different detector array positions, thus increasing the time required to collect one tomographic dataset by an even larger factor. Even under these difficult experimental conditions, the overall quality of the images is comparable to those of other small animal tomographic images available in the literature. This is mainly the result of the superior resolution capabilities of the BGO avalanche photodiode detectors used in this PET experiment.

Even with this small animal model, the axial resolution is sufficient to resolve the shape of an organ like the kidney, having dimensions of 7.3 × 10 × 6 mm, and to resolve the difference in the cephalo-caudal position of the two kidneys, the left one lying 0.5 cm caudal to the right one in a 150-g rat. This degree of resolution is one of the requirements for a suitable small animal tomograph (*7*). For quantitative work in which tracer concentrations must be measured accurately, it is well known that the resolution must be less than one-half the size of the object to be measured in order to avoid partial volume effects (*32*).

The data in Table 3 confirm that this requirement has been adequately satisfied for imaging of the rat, as the values obtained by PET and those obtained by the conventional dissection method for the kidneys and lungs are in agreement. The values obtained for the liver using the PET-based technique lie just outside those of the conventional method. The major discrepancy is for the tumor. However, this can be explained by the distribution of the [^{64}Cu]$CuPcS_4$ within the tumor. Sulfonated phthalocya-

TABLE 3
Comparison of Radioactivities in Various Organs as Determined by PET Imaging and by Dissection and Scintillation Counting One Hour After Injection

	^{64}Cu activity (μCi/mg)	
Tissue	PET imaging	Dissection and scintillation counting
Kidney	0.030 ± 0.003	0.021 ± 0.006
Liver	0.025 ± 0.004	0.017 ± 0.002
Lung	0.012 ± 0.002	0.012 ± 0.003
Tumor	0.011 ± 0.002	0.0016 ± 0.0001

nines are known to accumulate preferentially in the tumor's outermost layer which has the greatest degree of vascularization (*27*). Large tumors, because of poor vascularization become necrotic in the center and consequently have virtually no uptake in this region. In the scintillation counting measurement, the activity obtained for the tumor (Table 3) was averaged over the tumor's entire mass, including the very low uptake necrotic center. This obviously tends to decrease the observed value.

This difference in uptake is visible on closer inspection of the PET images. They show a higher concentration of $[^{64}Cu]CuPcS_4$ in the region of the tumor nearest the skin corresponding to the richest vascularization. The same distribution was also noted from the characteristic blue color distribution in the tumor during the dissection. The PET-based biodistribution measurement is based on this region of increased uptake, and reflects the actual tumoral tissue uptake. This simple fact demonstrates one of the advantages of PET: it is capable of revealing a nonuniform distribution within an organ, without a priori knowledge of the biodistribution and without modifications to the experimental protocol. Such refinement would be extremely tedious and time-consuming with the conventional techniques based on dissection and scintillation counting. It is worth noting that this fine structure information was obtained for an equivalent acquisition time for a full ring detector of only 4 min. With measurements of equivalent quality on this time scale, the determination of the time course of this particular distribution also becomes feasible.

This real time capability is lacking in recently proposed high-resolution pinhole (*33,34*) and slit (*35*) collimated SPECT-based approaches. Although the achievable resolution is excellent (~1.5 mm FWHM), the need, as with the Sherbrooke PET simulator, to reposition the detectors seriously limits the time resolution of each image. These approaches achieve high resolution at the expense of sensitivity. They nevertheless have a cost advantage as conventional SPECT systems and conventional tracers can be used. They do not permit, however, the use of metabolically important compounds labeled with positron emitting isotopes.

CONCLUSIONS

In conclusion, we have demonstrated the suitability of an avalanche photodiode detector-based PET imaging device for in vivo quantitation of tracer tissue distributions. The results obtained are compatible with dissection measurements and have a sufficiently high resolution and sensitivity to be used on small laboratory animals. With the current prototype PET system, sensitivity and acquisition speed are severely limited by the absence of a complete ring of detectors. Nevertheless, these preliminary data demonstrate that images of equivalent or superior quality can be obtained on a time scale sufficiently short for dynamic in vivo pharmacokinetic studies on small laboratory animals.

ACKNOWLEDGMENTS

The authors thank Huguette Savoie for assistance with tumor implantation and Michel Héon for help in image analysis. This work was supported by the Medical Research Council of Canada under grant MA-8549 and an MRC Group grant. Support is acknowledged from Le fonds de la recherche en santé du Québec (FRSQ) for a senior scholarship (RL) and studentships for initiation to health science research during the summer and the academic year (C.M.). Dr. Marriott was awarded the FRSQ Award of Excellence for summer students for this project.

REFERENCES

1. Agon P, Braeckman R, Van Haver D, Denutie H, et al. Drug distribution in dog brain studied by positron emission tomography. *Radiopharm Drug Disposition* 1988;9:567–577.
2. Fischman AJ, Livni E, Babich J, et al. Pharmacokinetics of ^{18}F-labeled fleroxacin in rabbits with Escherichia-Coli infection, studied with positron emission tomography. *Antimicrob Agents Chemother* 1992;36:2286–2292.
3. d'Argy R, Persson A, Sedvall G. A quantitative cerebral and whole body autoradiographic study of an intravenously administered benzodiazepine antagonist 3-H-Ro 15-1788 in mice. *Psychopharmacology* 1987;92:8–13.
4. Thorell JO, Stone-Elander S, von Holst H, Ingvar M. Synthesis of [1-^{11}C]-D-glucosamine and evaluation of its in vivo distribution in rat with PET. *Appl Radiat Isot* 1993;44:799–805.
5. Hume SP, Myers R, Bloomfield PM, et al. Quantitation of carbon-11-labeled raclopride in rat striatum using positron emission tomography. *Synapse* 1992;12:47–54.
6. Ingvar M, Eriksson L, Rogers GA, Stone-Elander S, Widén L. Rapid feasibility studies of tracers for positron emission tomography: high-resolution PET in small animals with kinetic analysis. *J Cereb Blood Flow Metab* 1991;11:926–931.
7. Miyaoka RS, Lewellen TK, Bice AN. Dynamic high resolution imaging of rats: design considerations. *IEEE Trans Nucl Sci* 1991;38:670–677.
8. Rajeswaran S, Bailey DL, Hume SP, et al. 2D and 3D imaging of small animals and the human radial artery with a high resolution detector for PET. *IEEE Trans Med Imag* 1992;11:386–391.
9. Watanabe M, Uchida H, Okada H, et al. A high resolution PET for animal studies. *IEEE Trans Med Imag* 1992;11:577–580.
10. Cutler PD, Cherry SR, Hoffman EJ, et al. Design features and performance of a PET system for animal research. *J Nucl Med* 1993;33:595–604.
11. Lightstone AW, McIntyre RJ, Lecomte R, Schmitt D. A bismuth germanate-avalanche photodiode module designed for use in high resolution positron emission tomography. *IEEE Trans Nucl Sci* 1986;NS-33:456–459.
12. Lecomte R, Martel C, Carrier C. Status of BGO-avalanche photodiode detectors for spectroscopic and timing measurements. *Nucl Instrum Meth Phys Res* 1989;A278:585–597.
13. Lecomte R, Cadorette J, Jouan A, Héon M, Rouleau D, Gauthier G. High resolution positron emission tomography with a prototype camera based on solid state scintillation detectors. *IEEE Trans Nucl Sci* 1990;37:805–811.
14. Héon M, Carrier C, Cadorette J, Richard P, Rouleau D, Rodrigue S, Lecomte R. A stationary sampling scheme for multi-layer positron tomographs. *IEEE Trans Med Imag* 1993;12:293–298.
15. Lecomte R, Cadorette J, Héon M, et al. Design and engineering aspects of avalanche photodiode PET tomograph. *1993 IEEE conference record: Nuclear science symposium and medical imaging conference*, volume 2. IEEE catalog no. 93CH3374-6;1993:1063–1067.
16. Scheuer J. Animal preparations relevant for study with positron emission tomography or nuclear magnetic resonance. *Circulation* 1985;72:IV139–IV144.
17. Harney JV, Wahl RL, Liebert M, et al. Uptake of 2-deoxy,2-(^{18}F)fluoro-D-glucose in bladder cancer: animal localization and initial patient positron emission tomography. *J Urology* 1991;145:279–283.
18. Daemen BJ, Elsinga PH, Paans AMJ, Wieringa AR, Konings AWT, Vaalburg W. Radiation-induced inhibition of tumor growth as monitored by PET using L-[1-^{11}C]tyrosine and fluorine-18-fluorodeoxyglucose. *J Nucl Med* 1992;33:373–379.
19. Daemen BJG, Elsinga PH, Ishiwata K, Paans AMJ, Vaalburg W. A comparative PET study using different ^{11}C-labeled amino acids in Walker 256 carcinosarcoma-bearing rats. *Nucl Med Biol* 1991;18:197–204.
20. Wilson BC, van Lier JE. Radiolabelled photosensitizers for tumor imaging and photodynamic therapy. *J Photochem Photobiol* 1989;3:459–463.

21. Mathias CJ, Welch MJ, Green MA, et al. In vivo comparison of copper blood-pool agents: potential radiopharmaceuticals for use with copper-62. *J Nucl Med* 1991;32:475–482.
22. Anderson CJ, Connett JM, Schwarz SW, et al. Copper-64 labeled antibodies for PET imaging. *J Nucl Med* 1992;33:1685–1691.
23. van Lier JE. Phthalocyanines as sensitizers for the PDT of cancer. In: Kessel D, ed. *Photodynamic therapy of neoplastic disease*, volume 1. Boca Raton, FL: CRC Press; 1990:279–291.
24. van Lier JE, Brasseur N, Paquette B, et al. Phthalocyanines as sensitizers for photodynamic therapy of cancer. *NATO ASI Series* 1988;H15: 435–444.
25. Rousseau J, Langlois R, Ali H, van Lier JE. Biological activities of phthalocyanines: synthesis, tumor uptake and biodistribution of ^{14}C-labeled disulfonated and trisulfonated gallium phthalocyanine in C3H mice. *J Photochem Photobiol B* 1990;6:121–132.
26. Rousseau J, Boyle RW, Maclennan AH, Truscott G, van Lier JE. Biodistribution and tumor uptake of [^{67}Ga]chlorogallium-tetraoctadecyloxy phthalocyanine and its sulfonation products in tumor bearing C3H mice. *Nucl Med Biol* 1991;18:777–782.
27. Rousseau J, Autenrieth D, van Lier JE. Synthesis, tissue distribution and tumor uptake of [^{99}Tc]tetrasulfophthalocyanine. *Int J Appl Radiat Isot* 1983;34:571–579.
28. Rousseau J, Ali H, Lamoureux G, LeBel E, van Lier JE. Synthesis, tissue distribution and tumor uptake of ^{99m}Tc- and ^{67}Ga-tetrasulfophthalocyanine. *Int J Appl Radiat Isot* 1985;36:709–716.
29. Scasnar V, van Lier JE. Biological activities of phthalocyanines—XV. Radiolabeling of the differently sulfonated ^{67}Ga-phthalocyanines for photodynamic therapy and tumor imaging. *Nucl Med Biol* 1993;20:257–262.
30. Weber JH, Busch DH. Complexes derived from strong field ligands: XIX. Magnetic properties of transition metal derivatives of 4, 4', 4", 4"'-tetrasulfophtalocyanines. *Inorg Chem* 1965;4:469–471.
31. Lecomte R, Cadorette J, Rodrigue S, et al. A PET camera simulator with multispectral data acquisition capabilities. *IEEE Trans Nucl Sci* 1993;40: 1067–1074.
32. Alpert NM, Barker WC, Gelman A, Weise S, Senda M, Correia JA. The precision of positron emission tomography: theory and measurement. *J Cereb Blood Flow Metab* 1991;11:A26–A30.
33. Erlandsson K, Ivanovic M, Strand SE, Sjögren K, Weber DA. High resolution pinhole SPECT for small animal imaging [Abstract]. *J Nucl Med* 1993;34:9P.
34. Jaszczazak RJ, Li J, Wang H, Zalutsky MR, Coleman RE. Pinhole collimation for ultra-high resolution small field of new SPECT studies [Abstract]. *J Nucl Med* 1993;34:10P.
35. Rogers WL, Slosar J, Hua L, Chiao P, Zhang Y, Clinthorne NH. A high resolution slit aperture for imaging small animals with SPECT [Abstract]. *J Nucl Med* 1993;34:9P.

EDITORIAL

Are Animal Scanners Really Necessary for PET?

For nuclear medicine not only to survive, but also to prosper, it must constantly seek out new radiopharmaceuticals that yield more information about tissue physiology than can be obtained by any other imaging modality. This process of radiopharmaceutical development is difficult, time-consuming and hindered by the lack of suitable instrumentation to facilitate evaluation of tracer pharmacokinetics (*1,2*).

Novel pharmaceuticals are routinely being developed at considerable cost. Human tumor lines have been successfully replicated in animals. Both these initiatives benefit from imaging procedures that can determine the interaction of drugs on regional metabolism, blood flow, and receptor occupancy and the extent of therapeutic intervention (*3*). Hence, radiopharmaceutical imaging is poised to play an even greater role in diagnosis, characterization and management of disease and dysfunction.

Two steps are entailed in the development of new radiopharmaceuticals that foster this approach: (1) synthesis and purification of a radiopharmaceutical, followed by (2) biodistribution and imaging studies to determine regional localization of the tracer. The easiest developmental path for new agents is by PET, since these agents are directly compatible with natural and man-made biomolecules. Incorporation of nuclides such as ^{13}N, ^{11}C and ^{18}F, is usually more straightforward than developing complex chelates from classical nuclear medicine nuclides such as ^{99m}Tc and ^{111}In. The short half-life of PET nuclides can be helpful when utilized for human studies (a lower patient dose is required and repeatability of imaging procedures is good), but they can also hinder successful tracer development (specific activity is reduced over time, rapid synthesis and quality assurance procedures are required, long incorporation times are not possible, and biodistribution studies are very difficult). But radiochemists have the ability to develop many more PET radiopharmaceuticals than can be thoroughly tested. Why? Quite simply, it takes too long to realistically evaluate whether a new radiopharmaceutical can be used to successfully visualize the desired physiological or biochemical parameter for which it was designed. Animal biodistribution studies must be performed for each new agent prior to undertaking human imaging (*4–6*). Numerous animals are required to gather limited amounts of kinetic data. The early uptake phase of a rapidly cleared tracer is difficult to measure by these techniques. Interanimal variability further increases the number of animals that must be killed. The cost and more importantly, the effort to collect biodistribution data for a few time points along this uptake process are significant, and become even more difficult when short half-life PET nuclides are used. Furthermore, conventional biodistribution methods of dissection provide no regional tissue uptake information.

In this issue of the *Journal* Marriott and coworkers present information about measuring biodistribution and regional uptake of PET radiopharmaceuticals in small animals (*7*). This builds upon their previous work (*8*) and employs avalanche photodiode detectors coupled to conventional BGO scintillator material. This work embodies two important issues, namely use of a dedicated small PET scanner for animal imaging and the development of new PET detector technology. The unique feature of their tomograph design is the application of the avalanche photodiode as the main

Received May 23, 1994; accepted May 23, 1994.
For correspondence or reprints contact: Richard Hichwa, Univ. of Iowa PET Imaging Center, Dept. of Radiology, Univ. of Iowa Hospital and Clinic, Iowa City, IA 52242.